Int J Adv Manuf Technol (2016) 86:2823–2835
DOI 10.1007/s00170-016-8359-0

ORIGINAL ARTICLE

Grinding process of helical micro-drill using a six-axis CNC grinding machine and its fundamental drilling performance

Suyan Zhang[1] · **Zhiqiang Liang**[1] · **Xibin Wang**[1] · **Tianfeng Zhou**[1] · **Li Jiao**[1] · **Pei Yan**[1] · **Hongchao Jian**[1]

Received: 6 October 2015 / Accepted: 13 January 2016 / Published online: 1 February 2016

Abstract Helical drill point is characterized by a continuous helical flank surface and an S-shape chisel edge, and its special geometry contributes to a superior drilling performance and a better grinding efficiency. However, the existing grinding processes are complicated and hard to be reproduced in practice, and it is difficult to meet the accuracy requirements as the drill diameter becomes smaller. Thus, it is crucial to research further grinding method of helical micro-drill and its drilling performance. In this paper, a grinding method of helical drill flank using a six-axis CNC grinding machine is proposed based on the mathematical model of generatrix of the helical surface. Then, this grinding process is simulated using the 3D CAD software and is validated by experimentally fabricating the helical micro-drill. The results show that this method is feasible for obtaining the micro-drill with high dimensional accuracy. For the comparison with helical micro-drill, the planar and conical micro-drills with the same geometry parameters are produced as well. The drilling experiments on 1Cr18Ni9Ti austenitic stainless steel with the planar, conical, and helical micro-drills are conducted, and the drilling force, tool wear, and hole quality are measured and analyzed. The experiment results show that the increasing rate of the radial force of helical micro-drills at the beginning of the drilling process is smaller than those of planar and conical micro-drills, the thrust force and wear of helical drill point are also smaller, and the quality of micro-holes by helical drill point is better as well. It is confirmed that the proposed grinding process is effective to fabricate the helical micro-drill with good drilling performance.

Keywords Micro-drill · Helical flank · Grinding process · Drilling performance

✉ Zhiqiang Liang
liangzhiqiang@bit.edu.cn

Suyan Zhang
zsyangela@sina.com

Xibin Wang
cutting0@bit.edu.cn

Tianfeng Zhou
zhoutf@bit.edu.cn

Li Jiao
jiaoli@bit.edu.cn

Pei Yan
pyan@bit.edu.cn

Hongchao Jian
kimi.chieh@126.com

[1] Key Laboratory of Fundamental Science for Advanced Machining, Beijing Institute of Technology, Beijing 100081, China

1 Introduction

Micro-hole drilling is a predominant operation in hole manufacturing industry and has been widely applied in various fields ranging from precision mechanics to advanced electronics, such as the production of automotive fuel injection nozzles, thick multi-layer printed circuit boards, air bearings, watches, and camera parts. [1]. There are many factors that influence the drilling performance including drill point geometry and drilling processing parameters. The drill point geometry is the most significant element in the micro-drilling process. Small variations in drill point geometry exert significant influence on the performance of the drill [2]. Therefore, many studies have been conducted to develop a better drill geometry to improve the drilling performance, such as conical [3], cylindrical [4], hyperbolic and ellipsoidal [5], and spiral, multi-facet drill point [6].

However, these conventional drill point geometries cannot be reproduced accurately on micro-drills due to its small physical size and the difficulty of fabrication process.

Nowadays, micro-drills with planar point geometry are widely used in the commercial markets, as its drill point grinding method is simple, effective, and economically applicable. Lin et al. [7] developed the general mathematical model and the grinding method for planar micro-drill points and investigated the characteristics of the drill. Then, this drill point model was further expanded by Lee et al. [8] in order to reduce the cutting force. However, this drill has a straight chisel edge shape and a low heel clearance angle distribution, which often lead to a high thrust force, high temperature, and fast tool wear. Furthermore, it is difficult to adjust the four flank surfaces to accurately intersect at one point, particularly when the drill diameter becomes smaller. To solve this problem, helical drill point for micro-drill was proposed and developed as an alternative [9, 10]. Its point characterized by a continuous helical surface and an S-shape chisel led to a superior drilling performance and a better grinding efficiency. In order to grind helical drill points, experimental grinding device with an assistant fixture was designed and assembled [11]. With this grinding machine, Ganglani and Ehmann [12] proved the feasibility of manufacturing helical drill points accurately with a computer-controlled servo system and controller. For the curved cutting edge of helicoid surface drill, Fetecau et al. [13] presented a toroidal grinding procedure and verified the feasibility of the method by grinding experiment. In order to improve the drilling quality and efficiency, Hsieh [14] proposed a mathematical model of the helical drill point which can be combined with the Denavit-Hartenberg notation, and then, the NC data for grinding the helical drill using a six-axis grinding machine was obtained by Hsieh [15] according to the ability matrix of the grinding machine and the configuration matrices of the grinding wheel.

The researches of drilling performance of helical drill point focused on the drilling force, tool wear, and geometry optimization, etc. In order to identify the best drill point geometry, Kang et al. [11, 16] compared the drilling performance of planar, conical, and helical drill points with diameter 7.45 mm in terms of cutting angle distribution, drilling torque and thrust, and skidding and wandering motion. The drill geometry affected burr formation greatly. Donfeld et al. [17] found that helical point drill produced much smaller burr than split point drill in Ti6Al4V drilling process. Jurko et al. [18] concerned on the tool wear and tool wear mechanisms by drilling of austenitic stainless steel with helical point drill. For the visualization design and optimization of helical drill, a numerical modeling and simulation CAD system was presented by Yan and Jiang [19] based on the helical drill model, and the geometric parameters could be modified reasonably according to different drilling requirements. Paul et al. [20] investigated the optimization of the shape of the drill point in order to minimize thrust and torque, and the point geometry

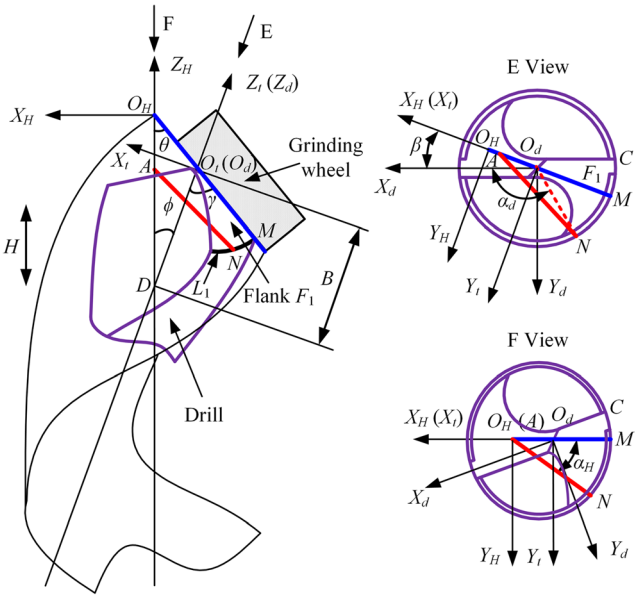

Fig. 1 The mathematical model of flank surface of helical drill point

was parameterized on the grinding parameters to ensure manufacturability of the optimized geometry.

However, the helical micro-drill is not widely appreciated and exploited, and its detailed investigation on the drilling performance is scanty, especially the helical point micro-drill with diameter less than 0.5 mm. Furthermore, the existing grinding processes are complicated and hard to be reproduced in practice, and it is difficult to meet the accuracy requirements as the drill diameter becomes smaller.

In this paper, the arbitrary position of the generatrix of helical surface is obtained firstly, and the generatrix mathematical model in the drill coordinate frame is developed. Then, the point coordinates and the direction of the generatrix in the machine coordinate system are determined, and a

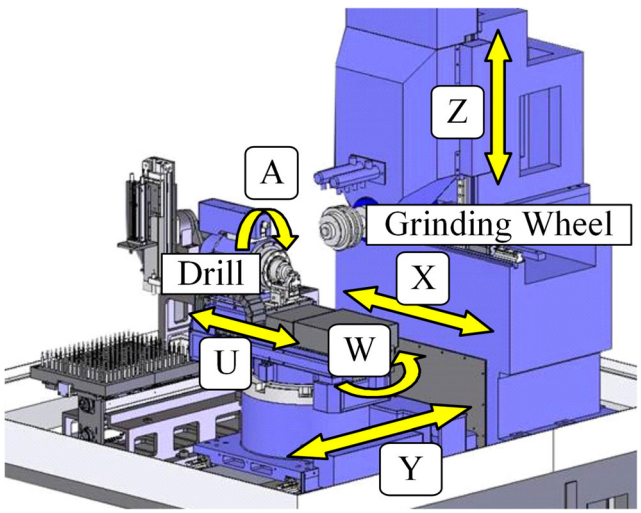

Fig. 2 The motion of Makino CNC grinding machine

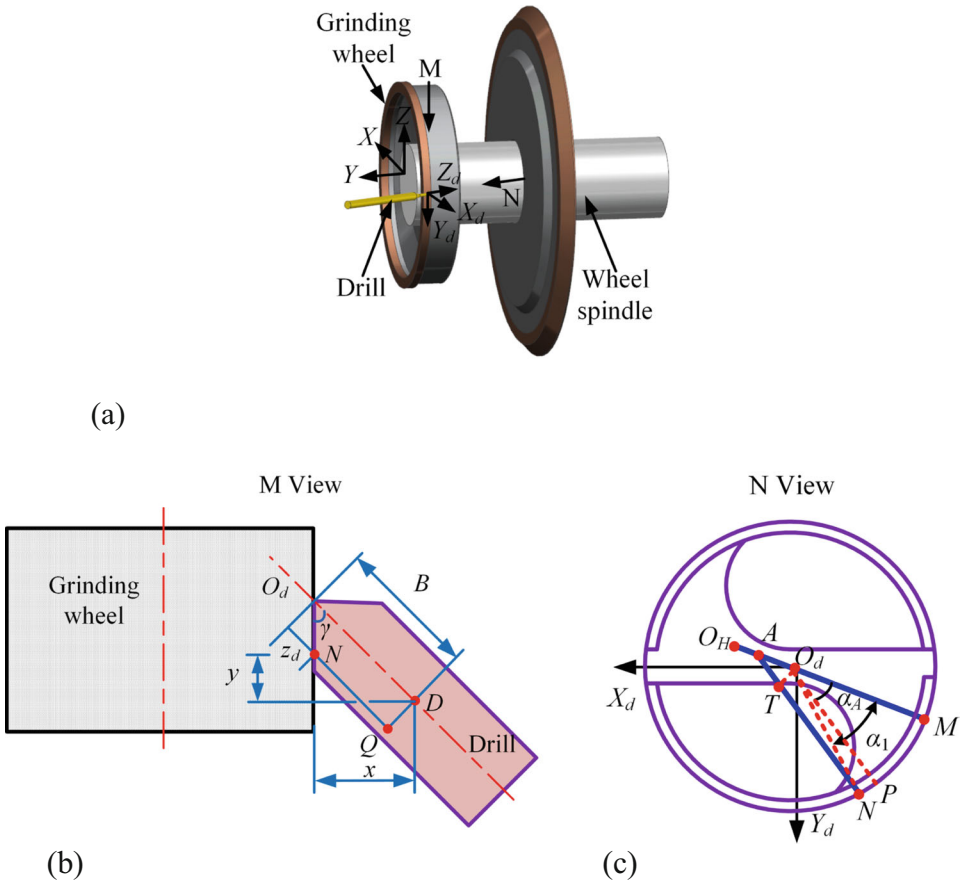

Fig. 3 Schematic diagram of the helical flank grinding process. **a** Relative position between drill and grinding wheel during grinding process. **b** Relative position in view M. **c** The motion of generatrix in view N

practical and efficient grinding method of helical drill flank using a six-axis CNC grinding machine is presented. Further, the grinding process is simulated using the 3D CAD software and is validated by fabricating the helical micro-drill with diameter 0.5 mm. For the comparison with helical micro-drill, the planar and conical micro-drills with the same geometry parameters are produced as well. For the fuel spray nozzle material 1Cr18Ni9Ti austenitic stainless, drilling experiments with planar, conical, and helical micro-drills are conducted, and the drilling force, the tool wear, and hole quality are measured and analyzed in order to investigate the helical micro-drill drilling performance.

2 Mathematical model of helical drill flank

Based on the mathematical model proposed by Lin et al. [9], the mathematical model of flank surface of helical drill point is shown in Fig. 1. The flank F_1 is made by part of the helical surface generated by the helical motion of generatrix O_HM along Z_H-axis. $X_HY_HZ_H$ is the coordinate frame of the helical surface. $X_dY_dZ_d$ is the coordinate frame built in the drill, with O_d locating at the drill tip, Z_d-axis coinciding with the drill axis, and the direction of X_d-axis positioning y-coordinate of the outer corner C ($y_c = -t$, $2t$ is web thickness). Rotating the O-$X_dY_dZ_d$ coordinate system around Z_d-axis by angle β, coordinate transformation system O-$X_tY_tZ_t$ is attained. Translating O_t to O_H by coordinate (x_0, y_0, z_0) and rotating the O-$X_tY_tZ_t$

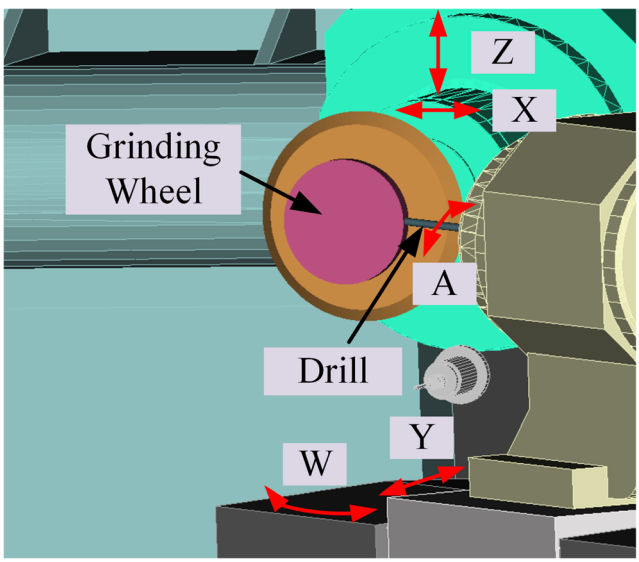

Fig. 4 The schematic illustration of the grinding operation

Table 1 The geometric parameters of the micro-drill

Geometric parameters	Drill diameter (mm)	Web thickness ratio	Helical angle of groove (°)	Semi-point angle ρ (°)	Chisel edge angle ψ (°)	Lip clearance angle α_{fc} (°)	Heel clearance angle $\alpha^{R}_{h,-60^\circ}$ (°)
Value	0.5	0.25	30	59	55	12	15

coordinate system around Y_t-axis by an angle of ϕ, helical coordinate frame O-$X_HY_HZ_H$ is attained. Apart from ϕ and β, there are three other parameters for grinding the helical flank, θ, H, and B, where B is the distance between the drill tip O_d and the intersection point D of Z_H-axis and Z_d-axis, H is the pitch of helical flank, and θ is the angle between grinding wheel surface and the Z_H-axis. The equation of the helical surface in $X_HY_HZ_H$ system can be expressed as follows:

$$F_1 : Z_H + \frac{\sqrt{X_H^2 + Y_H^2}}{\tan\theta} + \frac{H}{2\pi}\sin^{-1}\left(\frac{Y_H}{\sqrt{X_H^2 + Y_H^2}}\right) = 0 \quad (1)$$

By coordinate transformation, Trans(x_0, y_0, z_0), Rot(Y_H, $-\phi$), and Rot(Z_t, β), the equation can be transformed into the drill system $X_dY_dZ_d$.

$$\begin{aligned}&[X_H \;\; Y_H \;\; Z_H]^T \\ &= \mathrm{Rot}(Y_H, -\phi)\;\; \mathrm{Rot}(Z_t, \beta)\;\; [X_d \;\; Y_d \;\; Z_d]^T \\ &\quad + \mathrm{Trans}(x_0 \;\; y_0 \;\; z_0)\end{aligned} \quad (2)$$

where

$$\mathrm{Rot}(Y_H,\ \text{-}\phi) = \begin{bmatrix} \cos\phi & 0 & -\sin\phi \\ 0 & 1 & 0 \\ \sin\phi & 0 & \cos\phi \end{bmatrix}$$

$$\mathrm{Rot}(Z_t,\ \beta) = \begin{bmatrix} \cos\beta & \text{-}\sin\beta & 0 \\ \sin\beta & \cos\beta & 0 \\ 0 & 0 & 1 \end{bmatrix}$$

$$\mathrm{Trans}(x_0 \;\; y_0 \;\; z_0) = \begin{bmatrix} -B\sin\phi \\ 0 \\ -\dfrac{B\sin\phi}{\tan\theta} \end{bmatrix}$$

Then, the equation of helical flank in the system $X_dY_dZ_d$ can be expressed as follows:

$$\begin{aligned}&F_1 : Z_d\cos\phi - B\frac{\sin\phi}{\tan\theta} + \sin\phi(X_d\cos\beta - Y_d\sin\beta) \\ &\quad + \frac{\sqrt{[\cos\phi(X_d\cos\beta - Y_d\sin\beta) - \sin\phi(Z_d + B)]^2 + (Y_d\cos\beta + X_d\sin\beta)^2}}{\tan\theta} \\ &+ \frac{H}{2\pi}\sin^{-1}\left(\frac{Y_d\cos\beta + X_d\sin\beta}{\sqrt{[\cos\phi(X_d\cos\beta - Y_d\sin\beta) - \sin\phi(Z_d + B)]^2 + (Y_d\cos\beta + X_d\sin\beta)^2}}\right) \\ &= 0\end{aligned} \quad (3)$$

By rotating the grinding wheel around the Z_H-axis and simultaneously moving down along the Z_H-axis while drill is fixed, a helical surface is generated by the movement of the wheel [19]. However, the helical motion of the grinding wheel cannot be applied directly on a six-axis CNC tool grinder. Hence, the space composite motion of one object should be broken up into several planar motions of one or more objects. In order to achieve this, the arbitrary position of the generatrix during the helical motion will be obtained firstly, and then, the generatrix mathematical model of helical drill flank in the drill coordinate frame can be developed.

Assuming that line AN is the generatrix at one point, point N is on the intersecting line L_1 of the flank F_1 and the cylindrical surface of drill. The coordinate of point N in system $X_dY_dZ_d$, which is on the cylindrical surface of drill, can be described as $N_d(x_d, y_d, z_d) = [r\cos\alpha_d, r\sin\alpha_d, z_d] = [g_x(\alpha_d), g_y(\alpha_d), g_z(\alpha_d)]$, where r is the radius of drill, α_d is the angle between the line O_dN and X_d-axis, and z_d can be obtained by the Eq. 3 with variable α_d.

In the coordinate frame of the helical surface $X_HY_HZ_H$, suppose that the generatrix O_HM rotates angle α_H around Z_H-axis and simultaneously moves down along Z_H-axis to position AN, so the coordinate of point A in the system $X_HY_HZ_H$ is $A_H = \left[0,\ 0,\ -\frac{H}{2\pi}\alpha_H\right]$. By coordinate transformation Eq. 2, point A in the system $X_dY_dZ_d$ can be expressed as follows:

$$\begin{aligned}A_d &= \begin{bmatrix} x_a \\ y_a \\ z_a \end{bmatrix} = \begin{bmatrix} p_x(\alpha_H) \\ p_y(\alpha_H) \\ p_z(\alpha_H) \end{bmatrix} \\ &= \begin{bmatrix} \cos\beta\sin\phi\left(B\cos\phi - \dfrac{H}{2\pi}\alpha_H + B\dfrac{\sin\phi}{\tan\theta}\right) \\ -\sin\beta\sin\phi\left(B\cos\phi - \dfrac{H}{2\pi}\alpha_H + B\dfrac{\sin\phi}{\tan\theta}\right) \\ -B\sin^2\phi + \cos\phi\left(-\dfrac{H}{2\pi}\alpha_H + B\dfrac{\sin\phi}{\tan\theta}\right) \end{bmatrix}\end{aligned} \quad (4)$$

Table 2 The grinding parameters of helical drill flank

Grinding parameters	B (mm)	H (mm)	β (°)	θ (°)	ϕ (°)
Value	0.4964	0.9977	−3.1913	29.4869	30

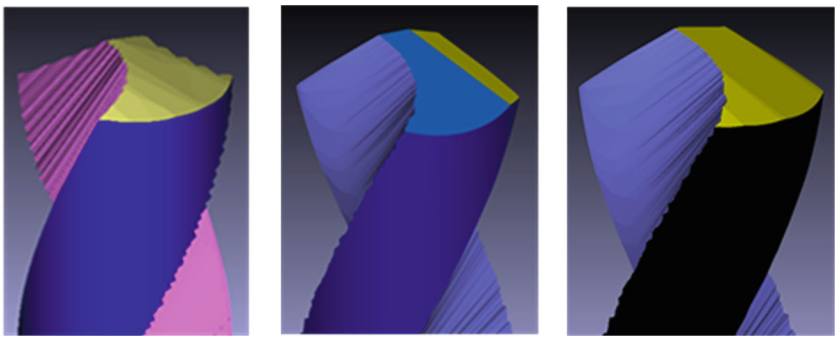

Fig. 5 The simulation results of the drills. **a** Helical drill point. **b** Planar drill point. **c** Conical drill point

Furthermore, the coordinate of point N in system $X_dY_dZ_d$ is $N_d(r\cos\alpha_d,\ r\sin\alpha_d,\ z_d)$. By coordinate transformation Eq. 2, the coordinate $N_H(x_H, y_H, z_H)$ in system $X_HY_HZ_H$ is as follows: $N_H(x_H,\ y_H,\ z_H) = [r\cos\phi\cos(\alpha_d+\beta)\text{-}(z_d+B)\sin\phi,\ r\sin(\alpha_d+\beta),\ z_H]$. So, α_H can be expressed by α_d as follows:

$$\alpha_H = f(\alpha_d) = \tan^{-1}\frac{y_H}{x_H} = \tan^{-1}\frac{r\sin(\alpha_d+\beta)}{r\cos(\alpha_d+\beta)\cos\phi-(B+z_d)\sin\phi} \tag{5}$$

Therefore, the coordinate of point A in system $X_dY_dZ_d$ can be expressed as $A_d(x_a,\ y_a,\ z_a) = [p_x(f(\alpha_d)),\ p_y(f(\alpha_d)),\ p_z(f(\alpha_d))] = [f_x(\alpha_d), f_y(\alpha_d), f_z(\alpha_d)]$ with variable α_d.

Thus, for arbitrary angle α_d, there is a certain generatrix AN, and the flank of helical drill can be expressed as a series of line determined by α_d. The function of line AN in the system $X_dY_dZ_d$ is as follows:

$$L_{AN}: \frac{x-g_x(\alpha_d)}{f_x(\alpha_d)-g_x(\alpha_d)} = \frac{y-g_y(\alpha_d)}{f_y(\alpha_d)-g_y(\alpha_d)} = \frac{z-g_z(\alpha_d)}{f_z(\alpha_d)-g_z(\alpha_d)} \tag{6}$$

3 Grinding process of helical drill flank

Helical point micro-drill is fabricated using a six-axis CNC grinding machine (CNS7d, by Makino Seiki Co., Ltd.). The configuration of the machine is shown in Fig. 2. During the

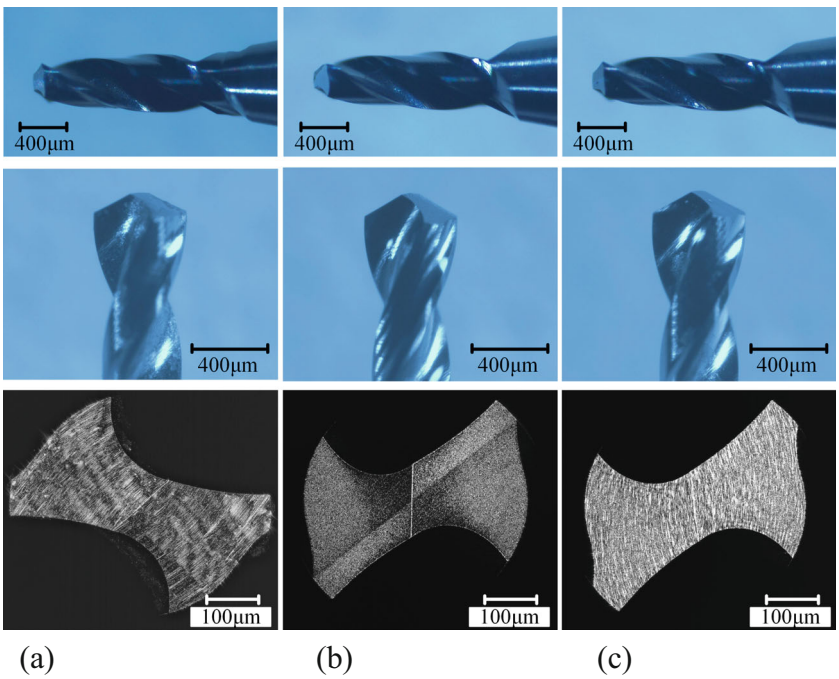

Fig. 6 The grinding experiment results of the micro-drills. **a** Helical drill point. **b** Planar drill point. **c** Conical drill point

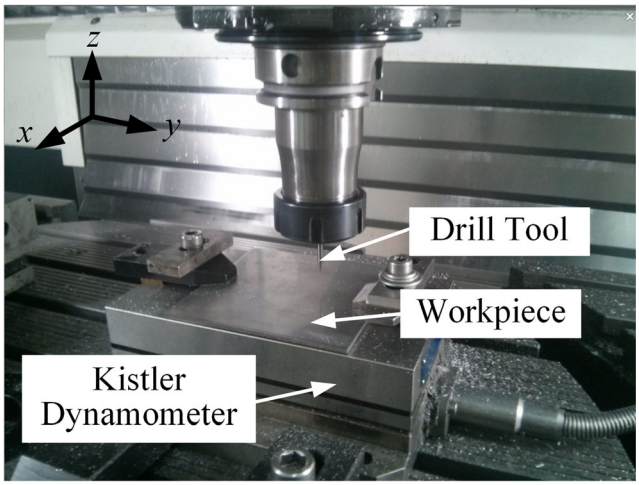

Fig. 7 The drilling experiment setup on DMG machining center

grinding process, the drill shank is clamped to make the drill axis coincide with A-axis, and the drill can move along U-axis and Y-axis, rotate about W-axis, while the grinding wheel can move along X-axis and Z-axis.

The relative position between the drill and the grinding wheel is shown in Fig. 3a during the generating of the helical flank, the cylinder surface of grinding wheel is used in this procedure, and the relation between grinding wheel and the drill can be seen as a line contact. To achieve the composite helical motion on the grinding machine, the arbitrary position of the generatrix L_{AN} in system $X_dY_dZ_d$ has been obtained in Sect. 2. Then, to ensure the contact line between grinding wheel and the drill is the certain generatrix AN, x, y, z coordinate of point N, and the direction of line AN in the machine coordinate system XYZ should be determined.

The direction of line AN in system $X_dY_dZ_d$ can be expressed as $\boldsymbol{AN}=(f_x(\alpha_d)-g_x(\alpha_d), f_y(\alpha_d)-g_y(\alpha_d), f_z(\alpha_d)-g_z(\alpha_d))$. In the machine system XYZ, it is determined by the machine movement shown in the view M and N. In the view M (Fig. 3b), the angle γ between the drill axis and the contact line L_{AN} can be derived from Eq. 6 as follows:

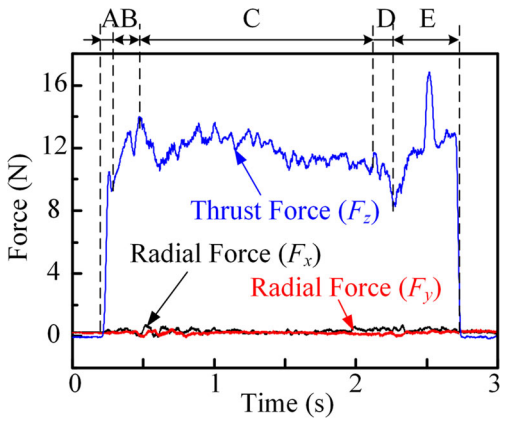

Fig. 8 Drilling force results of helical micro-drill with $v=22$ m/min and $f=0.002$ mm/r

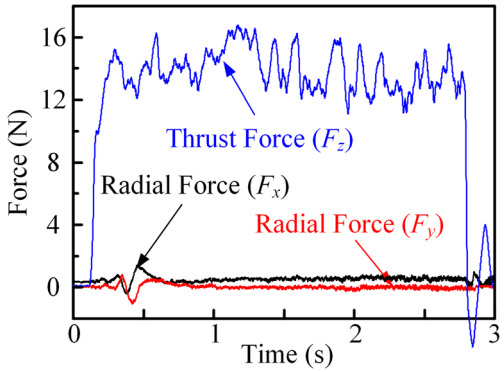

Fig. 9 Drilling force results of planar micro-drill

$$\gamma=\cos^{-1}\frac{f_z(\alpha_d)-g_z(\alpha_d)}{\sqrt{(f_x(\alpha_d)-g_x(\alpha_d))^2+\left(f_y(\alpha_d)-g_y(\alpha_d)\right)^2+(f_z(\alpha_d)-g_z(\alpha_d))^2}} \tag{7}$$

In the view N (Fig. 3c), blue lines represents the generatrices. Assuming that O_HM is the starting position of the generatrix, to arrive the next position AN, O_HM should rotate angle α_A around Z_d-axis and move distance O_dT along Z-axis. According Eqs. 4 and 5, the distance between point A and the drill tip O_d in the view N is as follows:

$$\begin{aligned}\left|\overline{O_dA}\right| &= \sqrt{f_x(\alpha_d)^2+f_y(\alpha_d)^2}\\ &= \left|\sin\varphi\left(B\cos\varphi-\frac{H}{2\pi}\tan^{-1}\left(\frac{r\sin(\alpha_d+\beta)}{r\cos(\alpha_d+\beta)\cos\phi-(B+z_d)\sin\phi}\right)+B\frac{\sin\varphi}{\tan\theta}\right)\right|\end{aligned} \tag{8}$$

In the triangle, AO_dN, $\left|\overline{O_dA}\right|/\sin(\alpha_1-\alpha_A)=r/\sin\alpha_A$. Based on sine theorem, α_A and $\left|\overline{O_dT}\right|$ can be expressed as follows:

$$\alpha_A=\tan^{-1}\left(\sin\alpha_1\Big/\left(\cos\alpha_1+\left|\overline{O_dA}\right|/r\right)\right),=\left|\overline{O_dA}\right|\cdot sin\alpha_A \tag{9}$$

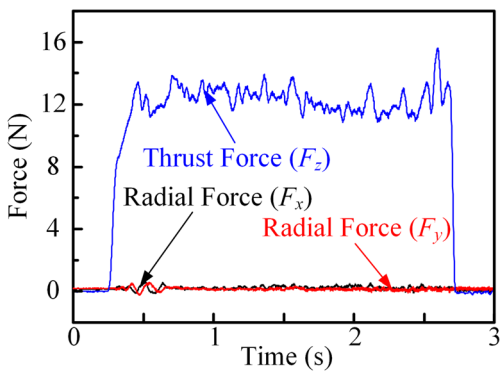

Fig. 10 Drilling force results of conical micro-drill

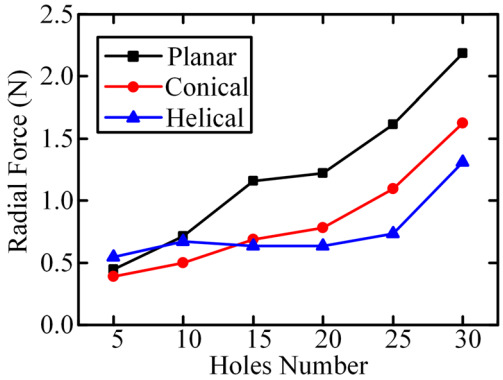

Fig. 11 The radial drilling force results at the beginning of the drilling process

where $\alpha_1 = \pi - \beta - \alpha_d$.

In order to make sure the direction of line AN, the rotation angle of W-axis is $\gamma + 90°$. For certain angle α_d, A-axis rotates angle α_A at the same time. Furthermore, Z-axis moves the distance $\left|\overline{O_dT}\right|$ to make sure the z coordinate of point N.

In the grinding process, U-axis moves distance B to make the rotation center of W-axis to be point D (shown in Fig. 1). Furthermore, in order to determine x, y coordinates of point N, the relative position (x_0, y_0) between point D and N is as follows:

$$x_0 = (B + z_d)\sin\gamma + \left|\overline{DQ}\right|\cos\gamma, y_0 = (B + z_d)cos\gamma - \left|\overline{DQ}\right|sin\gamma$$

$$\text{where } \left|\overline{DQ}\right| = \left|\overline{TN}\right|, \left|\overline{TN}\right| = \sqrt{\left|\overline{O_dT}\right|^2 + r^2} \quad (10)$$

4 Grinding simulation and experiment of helical micro-drills

To validate the proposed mathematical model and the corresponding grinding method, the simulation software MSPS of Makino Seiki grinding machine is used to simulate the motion of grinding procedure, and the schematic illustration of the grinding operation is shown in Fig. 4.

Based on the motion of this grinding machine, A-axis should rotate angle α_A, W-axis should rotate angle $\gamma + 90°$, and the grinding wheel should move along Z-axis by $\left|\overline{O_dT}\right|$. The drill should move along Y-axis, while the grinding wheel moves along the X-axis, to ensure the position of point N in the proper position. With the motion above, the helical drill flank can be generated accurately.

The geometric parameters of the helical drill point are listed in Table 1. The grinding parameter (θ, β, ϕ, B, H) of helical drill flank cannot be obtained uniquely according to the drill geometric parameters $\left(\rho, \psi, \alpha_{fc}, \alpha^R_{h,-60°}\right)$ due to grinding parameter redundancy [21]. The way to remove grinding parameter redundancy is to fix one of the grinding parameters. For the grinding method proposed in this paper, every grinding parameter is controllable. By considering the sensitivity of the grinding parameters, the most sensitive grinding parameter is identified as parameters ϕ. In this experiment, ϕ is set as 30°. To obtain the other grinding parameters, the least square method is used to solve the numerical results [21], and the grinding parameters of helical drill flank are listed in Table 2.

Based on these grinding parameters and grinding method above, the simulation software MSPS of Makino Seiki grinding machine is used to simulate the motion of grinding procedure and the simulation result is shown in Fig. 5a. Besides, the grinding experiment is carried out on the Makino Seiki six-axis CNC grinding machine, and the micro-drill is tungsten carbide tool. Then, the micro-drill is examined by 3D laser scanning microscope (VK-100 by Keyence Co., Ltd.), and the microscope photograph is shown in Fig. 6a. Meanwhile, the planar and conical micro-drills are fabricated on the six-axis CNC grinding machine with the same geometry parameters, and the simulation and experiment results are shown in Figs. 5b, c and 6b, c.

5 Drilling experiment of helical, planar, and conical micro-drills

To compare the drilling performances of the three kinds of drill points, drilling experiments are carried out on DMG

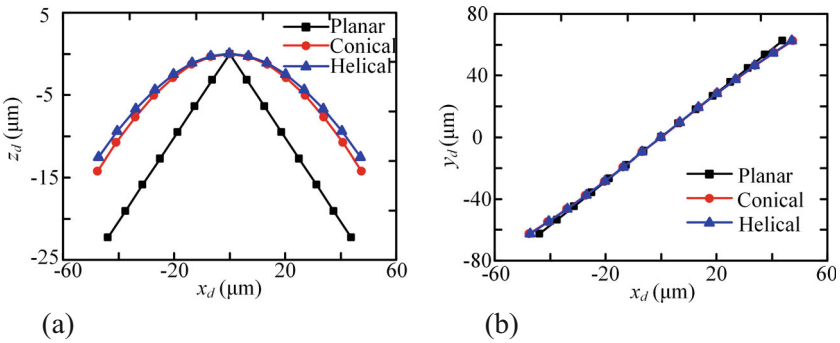

Fig. 12 Chisel edge shapes of helical, conical, and planar drill points. **a** Chisel edge shapes in X_d-Z_d plane. **b** Chisel edge shapes in X_d-Y_d plane

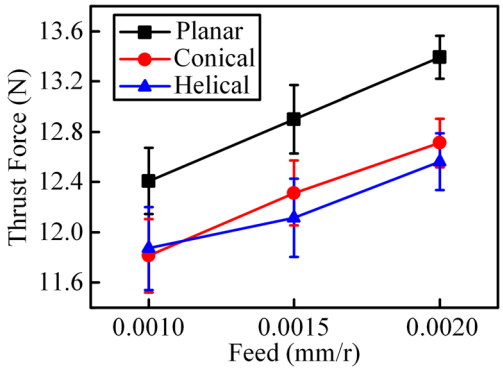

Fig. 13 The drilling force results of the helical, planar, and conical micro-drills

machining center (DMU80 monoBLOCK by DMG MORI Co., Ltd.), shown in Fig. 7. The workpiece material is 1Cr18Ni9Ti austenitic stainless steel. The drilling force is measured using a Kistler piezoelectric dynamometer model 9257B connected to a charge amplifier and data acquisition board, and the DynoWare (Kistler) is employed to collect the data.

5.1 Drilling force of helical, planar, and conical micro-drills

With rotational speed $n = 14000$ r/min and feed rate $f = 0.002$ mm/r, the drilling experiments of helical, planar, and conical micro-drills are carried out. Typical records obtained are shown in Figs. 8, 9, and 10, and the thrust force results clearly reveal the penetration phases.

In Fig. 8, in phase A, the micro-drill starts piercing into the workpiece, and the thrust force rapidly increases until the chisel edge has fully drilled into the workpiece. The thrust force increases continually during phase B, which is the cutting lip penetration period. After the chisel edge and the cutting lip have completely drilled into the workpiece, the thrust force is basically stable during phase C. When the chisel edge is close to the bottom of the stainless steel plate, the support rigidity for drill reduces. The thrust force decreases in phase D. In phase E, the drill point unthreads from the stainless steel plate and penetrates into the base plate. The drilling force variation tendency in Figs. 9 and 10 is in conformity with that in Fig. 8. However, the vibration of radial force F_x, F_y is serious in phases A and B for planar and conical micro-drills.

The amplitude of radial force at the beginning of the drilling process (phases A and B) is shown in Fig. 11. The chisel edge shapes in X_d-Y_d plane and X_d-Z_d plane are illustrated in Fig. 12 according to the coordinate definitions in Fig. 1, and they are calculated by the intersection of flank F_1 and its symmetrical flank with respect to Z_d-axis [9]. In Fig. 11, it shows that the radial force increases with the accruing of the hole number, and the growth trend for helical micro-drill is the slowest. At the beginning, the helical drill point may result in worse self-centering capability due to its larger chisel edge point angle (see Fig. 12a), the drill skidding and wandering motion is obvious, and the radial force of helical micro-drill is larger than the other. As the hole number increases, the chisel edge wear is gradually serious and it leads to more initial skidding and wandering; then, the radial drilling force increases. Furthermore, the sharp chisel edge for planar point micro-drill will be rapidly dulled after a few hits, and the radial drilling force increases faster due to the more serious wear phenomenon. However, the S-shape chisel edge of helical drill point (see Fig. 12b) will lead to better self-centering capability, and the radial drilling force increases slowly.

Under working conditions of $n = 14000$ r/min and $f = 0.001$, 0.0015, and 0.002 mm/r, the drilling experiments are carried out. The average drilling force in phase C of helical, planar, and conical micro-drills is shown in Fig. 13. The thrust force grows linearly with the increase of feed rate. Compared with the planar drill points, the helical and conical micro-drills produce a lower thrust force. The chisel edge plays an important role in the

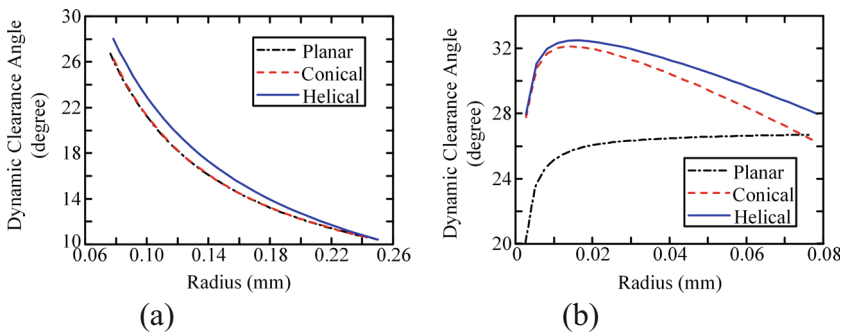

Fig. 14 Dynamic clearance angle comparisons along cutting lip and chisel edge with $f = 0.002$ mm/r. **a** The cutting lip. **b** The chisel edge

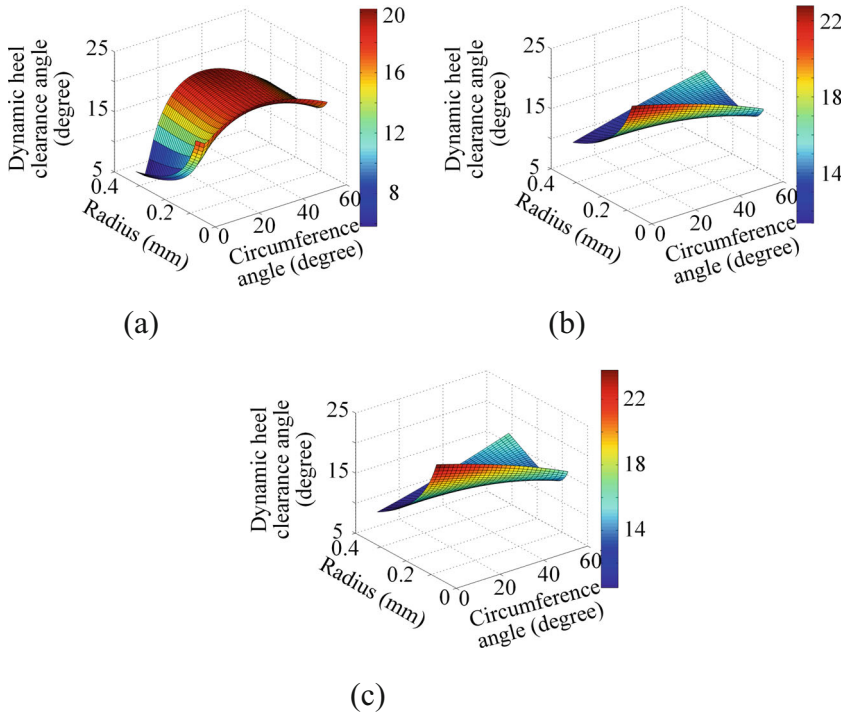

Fig. 15 Dynamic heel clearance angle distribution over the flank surface with $f = 0.002$ mm/r. **a** Planar drill point. **b** Conical drill point. **c** Helical drill point

drilling performance; it is an S-shaped curve for helical drill point which will lead to the reduced thrust force. Moreover, the clearance angle is an important factor during the drilling process, and its value should be larger near the center of the drill than at the outer corner to prevent the flank from rubbing. The dynamic clearance angle along the cutting lip and chisel edge and dynamic heel clearance angle distribution over the flank surface are shown in Figs. 14 and 15, and the calculation method was presented by Kang et al. [16]. For the helical micro-drill, the dynamic clearance angle is larger than the other, and it increases from the outer corner to the center of the drill. The dynamic heel clearance angle of helical micro-drill also keeps larger value over the flank surface, which results in smaller thrust force.

5.2 The wear of helical, planar, and conical micro-drills

Under the drilling condition that rotational speed $n = 14,000$ r/min and feed rate $f = 0.002$ mm/r, three drills of each type of drill points are taken to perform the drilling tests. Drill wear is measured using a 3D laser scanning microscope, and the method of wear measurement is shown in Fig. 16. After drilling 30 holes, microscope photograph of wear of planar, conical, and helical drill points and the magnification of flank and chisel edge wear are shown in Fig. 17. It can be seen that the wear of flank and chisel edge are obvious for the three types of micro-drills. Moreover, the flank wear of helical and conical micro-drills is less than that of planar micro-drill, and helical micro-drills have the least wear on chisel edge.

Figure 18 shows the value of chisel edge and flank wear. It is observed that the planar flank wear is the most serious, and the value of VB_{max} and C_{max} is larger than the other drill points. For the conical and helical drill points, the value of flank wear is basically equal to each other, but the wear phenomenon of chisel edge for conical drill point is severer than that of helical drill. It is clear that the chisel edge wear of helical drill point is

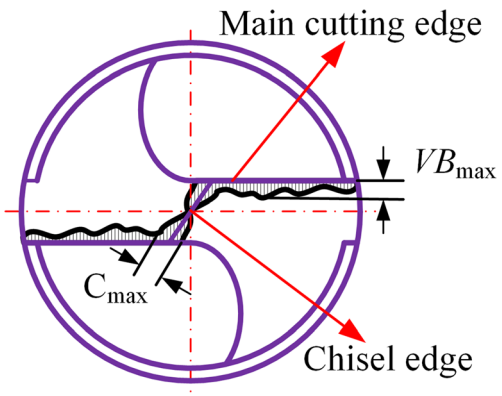

Fig. 16 Schematic diagram of wear measurement

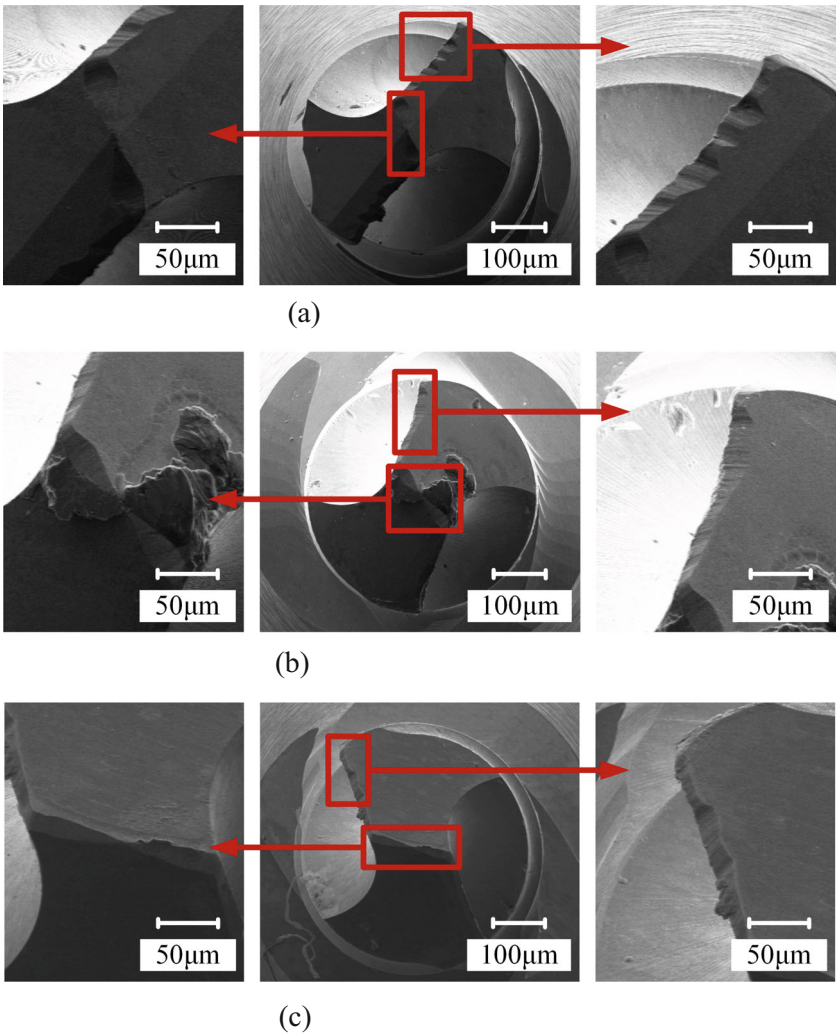

Fig. 17 Microscope photograph of wear of planar, conical, and helical micro-drills. **a** Planar micro-drill point. **b** Conical micro-drill point. **c** Helical micro-drill point

slight due to its smooth shape (see Fig. 12a), and the dynamic clearance angle distributions along the cutting lip and chisel edge for helical drill point are larger to prevent the flank from rubbing (see Fig. 14). Furthermore, for planar drill point, the very low heel clearance angle values are evident around the intersection line between the primary and secondary flank surfaces (Fig. 15a); these will cause a high thrust force, high temperature, and fast wear during the drilling process. As the drilling force plays an important role on the drill wear, the wear is slight for helical drill point due to the smaller drilling force, and then, the wear influences the drilling force as well.

5.3 Hole quality by helical, planar, conical and micro-drills

The micro-hole entrance morphology by planar, conical, and helical micro-drills is shown in Fig. 19. The roundness of micro-holes is measured using a 3D laser scanning microscope, and the method of roundness measurement is shown in Fig. 20. The roundness is the error between incircle radius R_1 and circumcircle radius R_2. Figure 21 shows the roundness value of micro-holes

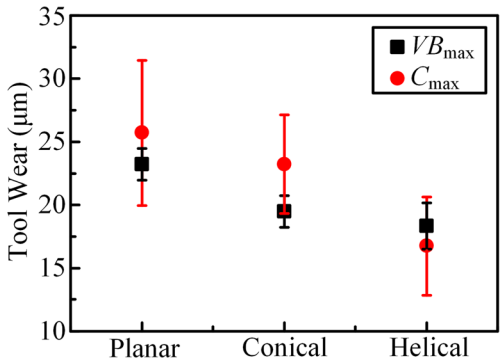

Fig. 18 Wear of chisel edge and flank of planar, conical, and helical micro-drills

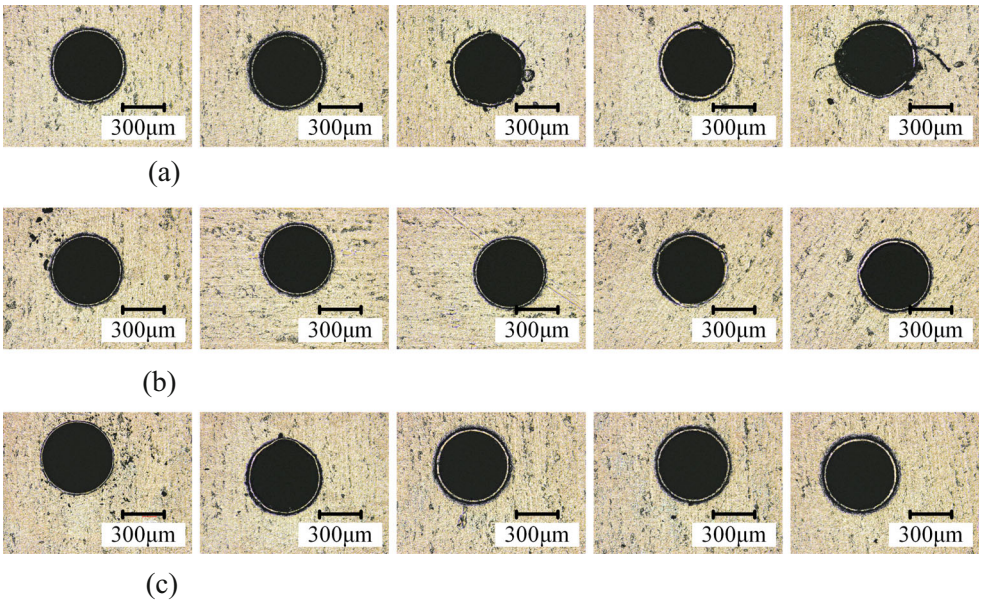

Fig. 19 The micro-holes by the planar, conical, and helical drill points. **a** The 6th, 12th, 18th, 24th, and 30th micro-holes by the planar drill point. **b** The 6th, 12th, 18th, 24th, and 30th micro-holes by the conical drill point. **c** The 6th, 12th, 18th, 24th, and 30th micro-holes by the helical drill point

by planar, conical, and helical drill points. It is observed that as the hole number increases, the micro-holes by planar drill point tend to be polygon, and the entrance morphology of micro-holes by helical drill point still keeps good quality. The roundness value becomes larger with the increased hole number, and the roundness of micro-holes by helical and conical drill points is better than that by planar drill point. It can be attributed to the radial force variation and chisel edge wear discussed in Sects. 5.1 and 5.2. As the hole number increases, the chisel edge wear is serious and the radial force increases. The increased radial force may lead to the larger roundness value. For the helical and conical micro-drills, the radial forces are smaller than those of planar micro-drill discussed in Sect. 5.1, resulting in better roundness of micro-holes.

The section morphology by planar, conical, and helical micro-drills is shown in Fig. 22. For the tenth micro-holes, the material spalling and scratch phenomenon appear by planar and conical drill points, and the phenomenon is more serious for the 20th micro-holes. Meanwhile, the slight scratch phenomenon appears by helical drill point for the 20th drilling holes. With the hole number increases, for the section morphology by the planar drill point, the burn happens due to the high temperature caused by the interference between the drill flank and the surface of the hole in the drilling process. In general, the surface quality of micro-holes by helical drill point is better than the others due to the smaller drilling force and drill wear.

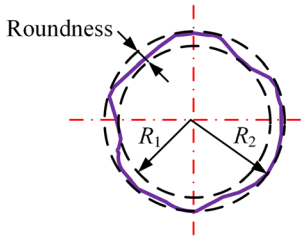

Fig. 20 Schematic diagram of roundness measurement

6 Conclusions

This paper proposes a mathematical model of generatrix of the helical surface, and presents a practical and efficient grinding method for fabricating helical drill flank using a six-axis CNC grinding machine. The helical micro-drills are fabricated using

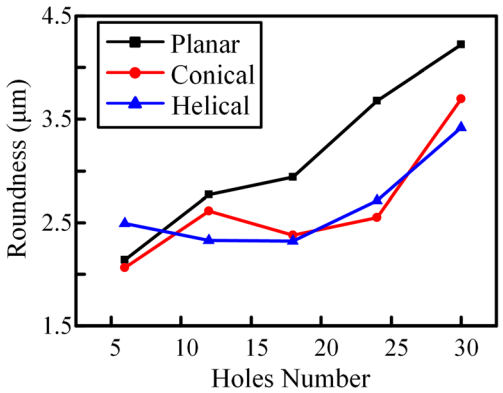

Fig. 21 The roundness of micro-holes

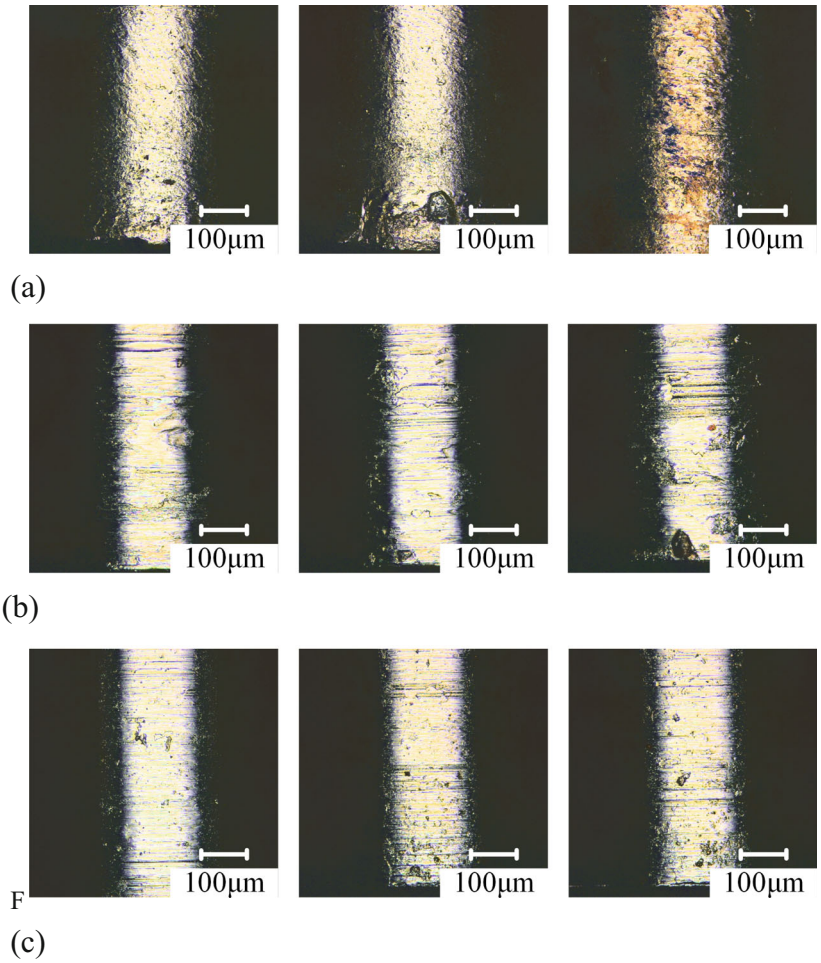

Fig. 22 The micro-hole section photograph by planar, conical, and helical drill points. **a** The 10th, 20th, and 30th micro-hole section photograph by planar drill point. **b** The 10th, 20th, and 30th micro-hole section photograph by conical drill point F. **c** The 10th, 20th, and 30th micro-hole section photograph by helical drill point

this grinding method, the planar and conical point micro-drills with the same geometry parameters are also produced. The 1Cr18Ni9Ti austenitic stainless steel drilling experiments with the three types of micro-drills are conducted, and the drilling force, the wear, and the hole quality are measured and analyzed. Some conclusions can be summarized as follows:

1. The grinding process is simulated using a 3D CAD software and is validated by experimentally fabricating the helical micro-drill, and the results show that this process is feasible for obtaining the micro-drill with high dimensional accuracy.
2. The increasing rate of the radial force of helical micro-drills at the beginning of the drilling process is smaller than those of planar and conical micro-drills, and this results in better entrance morphology of micro-holes.
3. The drilling thrust force and the wear of helical drill point are smaller due to the better chisel chip shape and dynamic clearance angle distribution, and the section morphology of micro-holes is better than those by planar and conical micro-drills.

This research validates that this grinding process is suitable to produce the helical micro-drill with less thrust force, less tool wear, and higher hole quality during the drilling process.

Acknowledgments This work was supported by the National Natural Science Foundation of China (No. 51575049, 51205024) and National Key Basic Research Program of China (No. 2015CB059900).

References

1. Galloway DF (1957) Some experiments on the influence of various factors on drill performance. Trans ASME 79:191–231
2. Chyan HC, Ehmann KF (1998) Development of curved helical micro-drill point technology for micro-hole drilling. Mechatronics 8(4):337–358
3. Fugelso MA (1990) Conical flank twist drill points. Int J Mach Tools Manuf 30(2):291–295
4. Fugelso MA (1983) Cylindrical flank twist drill points. ASME J Eng Ind 105(3):183–186
5. Tsai WD, Wu SM (1979) Computer analysis of drill point geometry. Int J Mach Tool Des Res 19(2):95–108
6. Wu SM, Shen JM (1983) Mathematical model for multifacet drills. ASME J Eng Ind 105(3):173–182

7. Lin C, Kang SK, Ehmann KF (1992) Planar micro-drill point design and grinding methods. Transactions of the North American Manufacturing Research Institution of SME XX:173–179
8. Lee AC, Nguyen DT, Wu GT (2014) Analyses of a new four-facet drill. Int J Adv Manuf Technol 75(1):411–424
9. Lin C, Kang SK, Ehmann KF (1995) Helical micro-drill point design and grinding. ASME J Eng Ind 117(3):277–287
10. Zhou ZX (2000) A kind of new micro-drill and grinding technology. PhD thesis, Hunan University, China
11. Kang SK (1993) Micro-drill geometry and grinding. PhD thesis, Northwestern University, USA
12. Ganglani S, Ehmann KF (2001) Design and implementation of a helical drill point grinder. Trans NAMRI/SME XX|X:1–8
13. Fetecau C, Stan F, Oancea N (2009) Toroidal grinding method for curved cutting edge twist drills. J Mater Process Technol 209(7): 3460–3468
14. Hsieh JF (2005) Mathematical model for helical drill point. Int J Mach Tools Manuf 45(7–8):967–977
15. Hsieh JF (2008) NC data generation for 6-axis machine tools to produce a helical drill. Int J Adv Manuf Technol 36(5):535–546
16. Kang SK, Lin C, Ehmann KF (1993) Comparative analysis of planar and helical micro-drill points. Trans NAMRI/SME XXI:189–196
17. Dornfeld DA, Kim JS, Dechow H, Hewsona J, Chenb LJ (1999) Drilling burr formation in titanium alloy, Ti-6AI-4V. CIRP Ann-Manuf Technol 48(1):73–76
18. Jurko J, Panda A, Behún M, Berdis A, Gecák J, Gecík M, Orendáč P (2012) Helical drills wear during drilling of a new ELC austenitic stainless steels. Appl Mech Mater 217–219:2202–2205
19. Yan L, Jiang F (2013) A practical optimization design of helical geometry drill point and its grinding process. Int J Adv Manuf Technol 64(9):1387–1394
20. Paul A, Kapoor SG, DeVor DE (2005) Chisel edge and cutting lip shape optimization for improved twist drill point design. Int J Mach Tools Manuf 45(4–5):421–431
21. Xiang WJ, Zhou ZX (2006) Analysis and solution of NC grinding parameter for new helical micro-drill point. Tool Eng 40(4):51–53